Nanoscale

Journal Name

ARTICLE

Atom Precise Platinum-Thiol Crowns

Anu George,[a] K. S. Asha,[a] Arthur C. Reber,[b] Scott R. Biltek,[c] Anthony F. Pedicini,[b] Ayusman Sen,[c]* Shiv N. Khanna,[b]* Sukhendu Mandal[a]*

Ligand stabilized water soluble Pt nanoclusters were synthesized and characterized through electrospray ionization mass spectrometry. Glutathione was used as the ligand, and $Pt_5(SG)_{10}$, and $Pt_6(SG)_{12}$ clusters were synthesized. Theoretical investigations found that these clusters do not possess a metal core, but rather are most stable in a ring structure. The clusters are stabilized through the thiol ligands forming a square planar structure around each Pt atom to form a ring. The structural elucidation was confirmed through UV/Vis and IR spectroscopy.

Introduction

One of the promising directions in the research on clusters is to synthesize materials whereby size selected clusters serve as the building blocks.[1] As the properties of clusters change with size and charged state, such assemblies offer the unique prospect of offering materials with tunable optical, electronic, magnetic and catalytic properties.[2–9] A key challenge in synthesizing such materials is that clusters are generally metastable and coalesce when brought together. One approach that ensures that the clusters remain separated is to use ligands and over the past decade there has been a tremendous effort in stabilizing ligated cluster assemblies. The ligands can exchange charge with clusters and also promote the formation of cluster assembled materials. In fact, a large number of such assemblies composed of Au_n, Ag_n, and mixed species ligated with a variety of ligands have been synthesized and characterized.[10,11] These assemblies contain clusters of precise size and composition that can be controlled by varying the experimental conditions. The resulting materials have shown novel optical properties, photoluminescence, magnetic properties, biocompatibility, and chemical properties that can be tuned with size.[4,12] Further, the materials are synthesized in solutions offering the possibility of large scale synthesis and often exhibit high resistance to chemical etching and oxidation. However, most of the assemblies have been confined to gold and silver based clusters and there have been only selected works on platinum, known to be an important

catalyst.[13] Tanaka and coworkers demonstrated the synthesis of dendrimer encapsulated fluorescent Pt nanoclusters (NCs) for bioimaging and subcellular targeting.[14] Navin et al. and Liu et al. employed matrix-assisted laser desorption ionization mass spectrometry (MALDI-MS) to characterize the Pt NCs capped with polyvinylpyrrolidone and 2-phenylethanethiol.[15,16] Duchesne et al. employed X-ray absorption spectroscopy to probe the local structure and electronic properties of Pt NCs reduced and stabilized using N, N-dimethylformamide.[17] Yamashina et al. have synthesized Pt_8 thiolates.[18] However, a complete structural and energetic analysis has not been achieved.

Herein we report a joint experimental and theoretical effort on the synthesis, structural characterization, optical absorption and electronic structure of ring-like Pt NCs stabilized by glutathione (GSH). To the best of our knowledge, this is the first attempt to theoretically predict the structure of Pt NCs. Glutathione protected clusters are well known for their solubility in water and for their stability compared to other thiolate clusters.[19] In a typical experiment, aqueous solutions of $H_2PtCl_6.H_2O$ (0.5 mmol) and L-reduced glutathione (1.5 mmol) were mixed together and stirred for 2 h at 0 °C. An ice-cold aqueous solution of $NaBH_4$ (3 mmol) was added drop wise under vigorous stirring. The solution was allowed to react for 4 h. A pale yellow solution was obtained which on precipitation with methanol gave a fine yellow powder. The as synthesized Pt:SG NCs were purified by repeated washing with methanol and dried for further characterizations (SG = deprotonated glutathione).

Methods

Materials.

All reagents were available commercially and used as purchased without further purification. Chloroplatinic acid hydrate (99.995 %), L- Glutathione reduced (≥ 98 %), Sodium

a. School of Chemistry, Indian Institute of Science Education and Research Thiruvananthapuram, Thiruvananthapuram, Kerala-695016, India.
b. Department of Physics, Virginia Commonwealth University, Richmond, VA, USA
c. Department of Chemistry, The Pennsylvania State University, University Park, PA, USA.
* Email: asen@psu.edu, snkhanna@vcu.edu, sukhendu@iisertvm.ac.in
† Photograph of the separation of the nanocluster using SEC. Isotopic distribution patterns of the nanocluster overlaid with the simulated one. EDX spectrum and the TEM image of the cluster, time dependent UV–vis spectra, TGA plot, IR spectrum and XPS spectrum and addition figures. See DOI: 10.1039/x0xx00000x

borohydride (99.99 %) and methanol (Chromasolv > 99.9%) were purchased from Sigma-Aldrich.

Methods.

ESI Mass spectrometric analysis was performed on a Waters LCT Premier time-of-flight (TOF) mass spectrometer. Operation of the mass spectrometer was performed using MassLynxTM software Version 4.0. Clusters were dissolved in deionized H_2O at concentration of 0.4 mg/mL and diluted 50% with methanol. Samples were introduced into the mass spectrometer using direct infusion via a syringe pump built into the instrument. The mass spectrometer was set to scan from 100-1800 m/z in negative mode, using electrospray ionization (ESI). The drying gas temperature was set to 120 °C, the source temperature was set to 100 °C and the capillary voltage was 2800 V.

The FT-IR spectrum was recorded from KBr pellets in the range of 4000-400 cm^{-1} on a Prestiage-21 SHIMADZU FT-IR spectrometer. The TGA was performed on SDT Q600 (Shimadzu) analyzer in flowing nitrogen with a heating rate of 10 ^{o}C per minute. UV-Vis spectroscopy was collected at room temperature on a UV-3800 SHIMADZU UV-Vis-NIR spectrometer. A Tecnai G2 F30 S-Twin transmission electron microscope (TEM) Operating voltage: 200 kV and FEI QUANTA-200 SEM. were used for the TEM and EDAX measurements.

Theoretical Methods.

Theoretical investigations were performed using the ADF[20] set of codes using the PBE exchange-correlation functional. The TZ2P basis set was used, with the ZORA approximation for relativistic effects.[22] Time Dependent-DFT calculations include 300 excitations and the line shape used was a Lorentzian with a Γ of 0.15 eV. We previously determined the structure of bimetallic clusters based on combined theoretical analysis and optical spectra.[23,24]

Results and Discussion

The crude product had a broad absorption spectrum which is indicative of the formation of a mixture of clusters.[25,26] Therefore the separation of these clusters was necessary to analyze their composition. The initial separation of these clusters was performed using size exclusion chromatography (SEC). The mixture separated into two bands (figure S1), where the smaller NCs moved slowly through the column and the larger clusters eluted quickly. The sample collected from the slow moving band was analyzed by electrospray ionization mass spectrometry (ESI-MS) in order to determine the molecular formula of any clusters present. This resulted in a spectrum with a particularly large number of peaks (figure S2). For the mass spectrum of any given cluster there will be a close grouping of peaks corresponding to the isotopic distribution in that cluster. There will then be a series of similar peak groupings corresponding to differing degrees of sodium exchange of the glutathione carboxylic acids. Finally each charge state of the cluster ions within the instrument will give rise to its own set of these series of peaks. In this

particular spectrum however it was clear that peaks were coming from more than one cluster, but since many of these peaks were at low intensity or had poor resolution they could not be clearly identified. In an attempt to better separate and fully characterize any clusters present we also decided to run the product through relatively low molecular weight cut off (MWCO) spin filters. For this purpose we used both 3k and 7k MWCO filters and analyzed the filtrate of both with ESI-MS (Figure 1). While the spectra of both show similar peak locations, there is an enhancement in the intensity of particular peaks in each. Based on peak positions, isotopic distributions, and the spacing between peaks, these peaks were assigned to a particular cluster with a particular charge state. The major peaks observed when the product was processed with a 3k MWCO filter can be assigned to Pt_5SG_{10} with -4, -5, and -6 charge states. The isotopic pattern of these peaks, centered at m/z = 1008, m/z = 806, and m/z = 672 respectively, matches well with the simulated spectra (figure 1 inset c, figure S3-4). When the product was processed with a 7k MWCO filter other peaks corresponding to larger molecular weights showed enhanced intensity. The clearest of these peaks, centered at m/z = 906 and m/z = 968 can be assigned to Pt_6SG_{11} and Pt_6SG_{12} respectively. These peaks are in the -5 charge state and match well with the simulated spectra[20] (figure 1 inset b, figure S5). It is important to note that the Pt_6SG_{11} peak may well be the result of fragmentation of the Pt_6SG_{12} cluster within the mass spectrometer, particularly since the simulated spectrum only truly matches well for an intrinsically positively charged $Pt_6SG_{11}^+$ which has lost 6 protons by ionization $[Pt_6SG_{11}-6H]^{5-}$, giving it the final charge of -5. Some peaks had poor intensity and resolution and therefore could not be properly identified. Considering solely their peak positions it is likely the majority of these are simply different charge states of the clusters identified above, although the possibility of other similarly sized clusters cannot be discounted. The chemical compositions of the Pt NC were analyzed using an energy dispersive X-ray spectroscopy (EDAX), (figure S6).
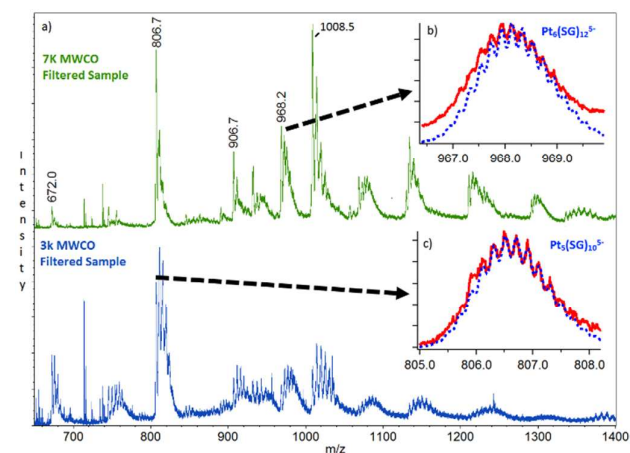

Figure 1. a) ESI-MS spectrum of Pt nanocluster samples purified with 7k MWCO (top) and 3k MWCO (bottom) filters. Inset shows the experimental mass spectra overlaid with simulations of b) $[Pt_6SG_{12}-5H]^{5-}$ and c) $[Pt_5SG_{10}-5H]^{5-}$. Note: All experimental plots were shifted by -0.1 m/z to match simulations. We believe

this mismatch was caused by a very small instrumental calibration error, only noticeable because of the high charge states of the cluster ions. Additional peak fits are provided in the SI.

The as synthesized clusters were highly soluble in water. Figure 2 shows the UV-vis absorption spectrum of Pt NC in water. The cluster shows a broad absorption feature around 300 nm. Pure GSH has an absorption in the 200-250 nm window. Reduction of Pt(IV) to Pt(II) on the formation of the nanocluster was confirmed from the change in colour, figure S7a. Notably, the clusters show the same absorption profile even after several months of storage in the refrigerator in aqueous solution and in the solid state without the protection of inert gas which suggests high stability as determined by the time-resolved optical absorption spectroscopy, figure S7b. The thermal stability of the cluster was verified using thermo-gravimetric analysis (TGA), figure S8. The nanocluster is stable at room temperature, but is unstable at higher temperatures.
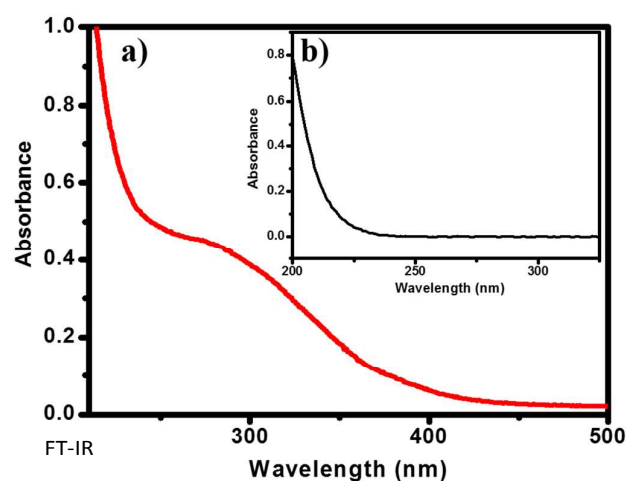

Figure 2. a) UV- Vis spectrum of Pt nanoclusters. Inset b) Absorption profile of pure GSH.

FT-IR spectroscopy was utilized to gain further insight into the chemical and surface properties of the prepared Pt NC, figure 3. The purified Pt cluster exhibited characteristic pattern of vibrational stretching frequency implying the presence of ligands residing on the nanocluster surface. The peak at 2526 cm^{-1} in the glutathione spectrum which corresponds to S-H stretching vibration mode disappears in the vibrational spectrum of Pt NC. This provides the evidence for the cleavage of the S-H bond and binding of the ligand onto the Pt surface through Pt-S bonding. The oxidation state of Pt was then investigated using X-ray photoelectron spectroscopy (XPS) measurements, figure S9. The electron binding energy value for Pt $4f_{7/2}$ is ~72.3 eV, which is higher than the binding energy value of Pt (0). Therefore, the oxidation state of the obtained Pt cluster is not Pt (0) suggesting the presence of a crown-like structure and the absence of metallic core.
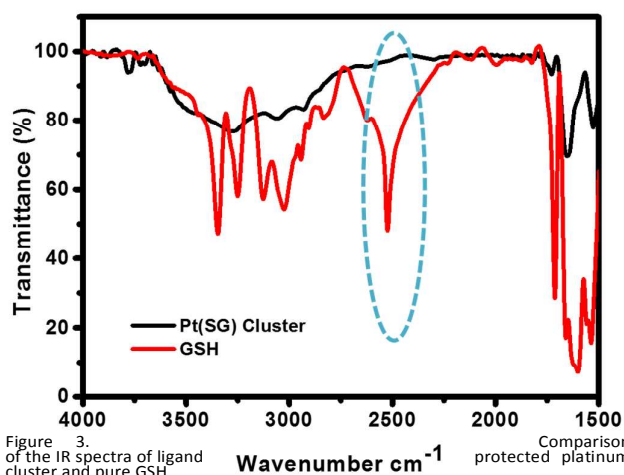

Figure 3. Comparison of the IR spectra of ligand protected platinum cluster and pure GSH.

Theoretical investigations using gradient corrected density functional theory[20,21] were performed to determine the structure of the $Pt_n(SR)_{2n}$ clusters. The lowest energy structures for n=5, and 6 are shown in Figure 4, and the structures for n=1-8 are shown in figure S10. We have used SCH_3 in place of glutathione, to reduce the computational cost. The lowest energy structures are ring structures with each Pt atom surrounded by four S atoms in a square planar configuration. For $Pt_6(SCH_3)_{12}$, a cage isomer lies 0.14 eV higher in energy than the ring structure, figure S11. The optimal geometries have two Pt-S bonds per thiol ligand, and 4 per Pt atom. The stability is affected by the strain in the square planar arrangement of thiol ligands around the Pt atom, and for this reason the ring structure is slightly more stable. Glutathione is much bulkier than the methyl group used in our calculations, and this will further decrease the stability of the cage structure.
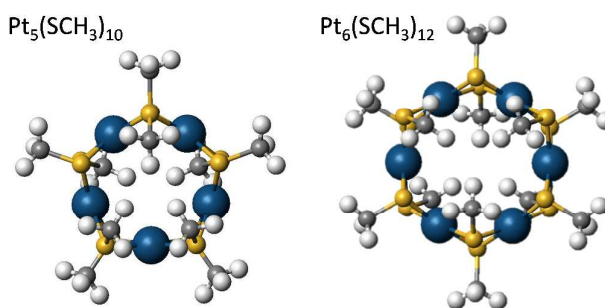

Figure 4. Lowest energy structures calculated for $Pt_5(SCH_3)_{10}$, and $Pt_6(SCH_3)_{12}$.

The square planar structure of the $Pt_n(SR)_{2n}$ clusters results in the clusters being electronically stable with the Pt atom having a $5d^8$ electronic configuration. The HOMO-LUMO gap of the n=5 and 6 clusters are 2.38 eV and 2.67 eV, respectively.

The HOMO-LUMO gap energy, and the binding energies are shown in Figure 5a. The binding energy is calculated using Eq. 1.

$$\frac{BE}{Unit} = \frac{\left(nE(Pt) + 2nE(SCH_3) - E(Pt_n(SCH_3)_{2n}\right)}{3n} \quad \textbf{Eq. (1)}$$

We find that the HOMO-LUMO gap increases from n=1-6, after which the gap remains approximately constant for n=6-8. The binding energy per unit are shown in Figure 5a, and shows that n=1-3 are relatively unstable, and that a plateau is reached at $Pt_6(SCH_3)_{12}$. This increase in binding energy is due to the decreasing strain on the square planar configuration of the ligands. The HOMO-LUMO gap for $Pt_4(SR)_8$ is 2.02 eV, and the short S-Pt-S angle is 78.5°, versus 81.2° and 81.5° in $Pt_6(SR)_{12}$, and $Pt_8(SR)_{16}$ respectively, indicating that there is still some strain in the structure. This helps to explain why $Pt_5(SR)_{10}$, and $Pt_6(SR)_{12}$ are the most abundant species in the mass spectra.
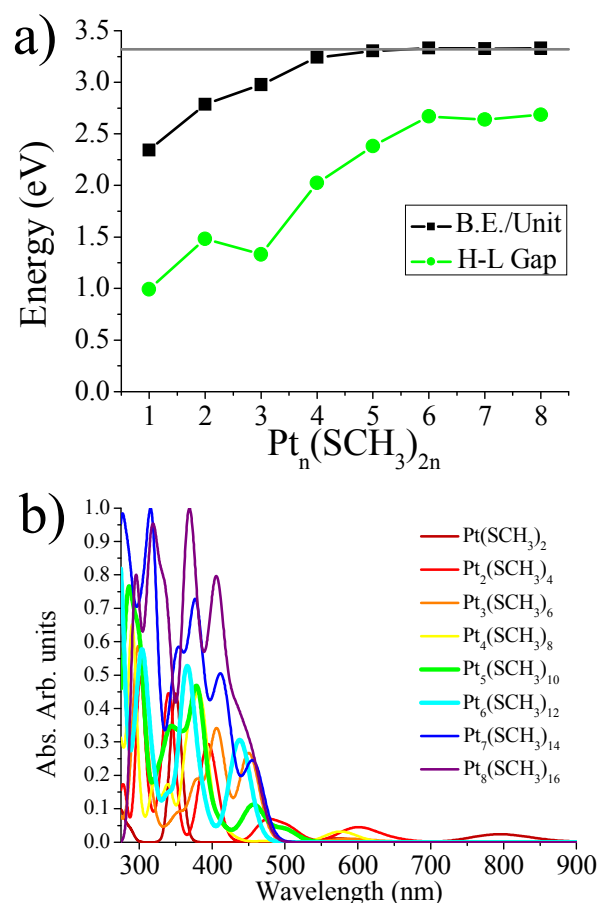

Figure 5. a) HOMO-LUMO gap, and Binding energy per Pt atom and SCH_3 ligand with the gray line fixed at 3.32 eV, the average value for n=6-8. b) Calculated optical absorption spectra of $Pt_n(SCH_3)_{2n}$, n=1-8.

Next, to confirm ring structure of the cluster we have examined the calculated optical absorption spectra of $Pt_n(SCH_3)_{2n}$, n=1-8 in Figure 5b. The lowest energy absorption peak for $Pt_5(SCH_3)_{10}$ is found to be 506 nm, and the lowest energy absorption peak of $Pt_6(SCH_3)_{12}$ is found to be 462 nm. The absorption peaks are somewhat lower in energy than the experimental absorption measurement, although density functional theory typically underestimates the band gap. Spin

orbit effects may also affect the calculated spectra. The absorption spectra generally blue-shifts with increasing size, until $Pt_6(SCH_3)_{12}$ at which point the HOMO-LUMO gap and absorption spectra have similar energy onsets. The absorption peaks are 5d-5d transitions in the platinum atom, and are localized on the atom. For this reason, we do not expect the replacement of glutathione with methyl groups to significantly affect the lowest energy optical transitions.

Conclusions

We have reported the synthesis, structural elucidation of water soluble platinum-glutathione clusters and identified $Pt_5(SG)_{10}$, and $Pt_6(SG)_{12}$ as air stable atom-precise clusters. These clusters have been characterized with electrospray mass spectrometry. Theoretical investigations find that these clusters have ring structures and their high stability is due to the square planar configuration of the thiol ligands around each Pt atom, resulting in large crystal field splitting in the 5d orbitals, with Pt having $5d^8$ electronic configuration. The cleavage of the S-H bond is confirmed by IR spectroscopy and the calculated optical spectra show reasonable agreement with the experimental spectra. Furthermore, this cluster can be synthesized in large quantities and its platinum sites make it a promising species for additional studies of catalytic properties.

Acknowledgements

Notes and references

1 S. A. Claridge, A. W. Castleman, S. N. Khanna, C. B. Murray, A. Sen and P. S. Weiss, *ACS Nano*, 2009, **3**, 244–255.
2 S. Sivaramakrishnan, P.-J. Chia, Y.-C. Yeo, L.-L. Chua and P. K.-H. Ho, *Nat. Mater.*, 2007, **6**, 149–155.
3 T.-H. Lee, J. I. Gonzalez, J. Zheng and R. M. Dickson, *Acc. Chem. Res.*, 2005, **38**, 534–541.
4 Y. Zhu, H. Qian, B. A. Drake and R. Jin, *Angew. Chem. Int. Ed.*, 2010, **49**, 1295–1298.
5 X. Liu, F. Wang, A. Niazov-Elkan, W. Guo and I. Willner, *Nano Lett.*, 2013, **13**, 309–314.
6 B. Panigrahy, M. Aslam and D. Bahadur, *Nanotechnology*, 2012, **23**, 115601.
7 J. Xie, Y. Zheng and J. Y. Ying, *J. Am. Chem. Soc.*, 2009, **131**, 888–889.
8 C.-A. J. Lin, T.-Y. Yang, C.-H. Lee, S. H. Huang, R. A. Sperling, M. Zanella, J. K. Li, J.-L. Shen, H.-H. Wang, H.-I. Yeh, W. J. Parak and W. H. Chang, *ACS Nano*, 2009, **3**, 395–401.
9 S. Mandal, A. C. Reber, M. Qian, P. S. Weiss, S. N. Khanna and A. Sen, *Acc. Chem. Res.*, 2013, **46**, 2385–2395.

10 J. Zheng and R. M. Dickson, *J. Am. Chem. Soc.*, 2002, **124**, 13982–13983.

11 H. Duan and S. Nie, *J. Am. Chem. Soc.*, 2007, **129**, 2412–2413.

12 M. Zhu, C. M. Aikens, F. J. Hollander, G. C. Schatz and R. Jin, *J Am Chem Soc*, 2008, **130**, 5883–5885.

13 K. An, S. Alayoglu, N. Musselwhite, K. Na and G. A. Somorjai, *J. Am. Chem. Soc.*, 2014, **136**, 6830–6833.

14 S.-I. Tanaka, J. Miyazaki, D. K. Tiwari, T. Jin and Y. Inouye, *Angew. Chem. Int. Ed.*, 2011, **50**, 431–435.

15 J. K. Navin, M. E. Grass, G. A. Somorjai and A. L. Marsh, *Anal. Chem.*, 2009, **81**, 6295–6299.

16 C. Liu, G. Li, D. R. Kauffman, G. Pang and R. Jin, *J. Colloid Interface Sci.*, 2014, **423**, 123–128.

17 P. N. Duchesne and P. Zhang, *Nanoscale*, 2012, **4**, 4199–4205.

18 Y. Yamashina, Y. Kataoka and Y. Ura, *Inorg. Chem.*, 2014, **53**, 3558–3567.

19 Y. Negishi, K. Nobusada and T. Tsukuda, *J. Am. Chem. Soc.*, 2005, **127**, 5261–5270.

20 G. te Velde, F. M. Bickelhaupt, E. J. Baerends, C. Fonseca Guerra, S. J. A. van Gisbergen, J. G. Snijders and T. Ziegler, *J. Comput. Chem.*, 2001, **22**, 931–967.

21 J. P. Perdew, K. Burke and M. Ernzerhof, *Phys. Rev. Lett.*, 1996, **77**, 3865–3868.

22 E. van Lenthe, A. Ehlers and E.-J. Baerends, *J. Chem. Phys.*, 1999, **110**, 8943–8953.

23 S. R. Biltek, S. Mandal, A. Sen, A. C. Reber, A. F. Pedicini and S. N. Khanna, *J. Am. Chem. Soc.*, 2013, **135**, 26–29.

24 S. R. Biltek, A. Sen, A. F. Pedicini, A. C. Reber and S. N. Khanna, *J. Phys. Chem. A*, 2014, **118**, 8314–8319.

25 K. G. Stamplecoskie, P. V. Kamat, *J. Am. Chem. Soc.*, 2014, **136**, 11093–11099.

26 S. Kumar, M. D. Bolan, T. P. Bigioni, *J. Am. Chem. Soc.*, 2010, **132**, 13141–13143.

Nanoscale Accepted Manuscript